

Generalized two-dimensional mesoscopic quantum transport: Application to disordered quantum wires

I. Vurgaftman and J. R. Meyer

Code 5613, Naval Research Laboratory, Washington, DC 20375

(Received 31 July 1996; revised manuscript received 29 October 1996)

A two-dimensional (2D) finite-difference time-domain model based on wave-packet propagation has been formulated. This method, which is capable of treating arbitrary potential profiles, is applied to the problem of finding the momentum (k) relaxation rates for each subband due to interface roughness scattering in disordered quantum wires as a function of wire width, electron energy, disorder correlation length (Λ), and disorder penetration depth. Results from the general 2D numerical approach are compared with those from 1D calculations based on the adiabatic approximation and the Born approximation. The error introduced by the Born approximation is found to be as much as a factor of 2.5 for small correlation lengths ($\Lambda k < 1$), and becomes significantly greater for large correlation lengths ($\Lambda k \gg 1$) owing to the predominance of higher-order scattering processes. If only intrasubband scattering is effective, the adiabatic approximation agrees to within 50% with the more general 2D results for a wide range of disorder parameters. However, the relaxation time decreases significantly at higher energies with the onset of scattering to higher electron subbands, which the adiabatic approximation is incapable of treating. For electron energies lower than the average disorder-induced potential barriers, the electron wave packet becomes localized with slow probability density decay due to tunneling. [S0163-1829(97)09107-8]

I. INTRODUCTION

The recent progress in nanofabrication techniques has created interesting opportunities for studying quantum transport phenomena in semiconductor mesoscopic systems. In view of the increasing complexity of nanostructures now being fabricated, analytic modeling approaches based on idealized geometries have become inadequate, and more general theoretical methods are needed. As a step toward this goal, here we discuss the development of a quantum transport calculation based on a numerical solution of the time-dependent two-dimensional (2D) Schrödinger equation, which can in principle be applied to mesoscopic device structures with arbitrary lateral geometries.

To illustrate its application, we will calculate momentum relaxation times for quantum wires with randomly fluctuating widths. Although the lateral substructure is unintentional in this example, nonetheless it will be seen that for most conditions of interest it is important to treat the transport in a fully two-dimensional context rather than as a perturbed one-dimensional problem. The potentially interesting carrier transport properties in quantum wires were first noted some time ago with the prediction that ionized impurity scattering in quantum wires can be dramatically suppressed owing to the reduction to one electronic degree of freedom.¹ Therefore, at low temperatures electrons in quantum wires could in principle exhibit very high mobilities, which would ultimately be limited by scattering from fluctuations in the position of the potential barrier interfaces. Since then a number of approaches to fabricating quantum wires with heterostructure barrier confinement has been developed. Among the most important are lateral patterning,²⁻⁵ and growth on vicinal^{6,7} and patterned nonplanar substrates,^{8,9} which yield differing degrees of interface quality. The importance of in-

terface roughness scattering in quantum wires has recently been confirmed experimentally.^{4,10}

The roughness-limited mobility in quantum wires has most often been studied within the Born approximation¹¹ by analogy with the treatment of this scattering mechanism in quantum wells.¹² However, it has been pointed out recently that for carrier densities greater than $\approx 10^6 \text{ cm}^{-1}$, the Born approximation can underestimate the scattering rate by many orders of magnitude, because the contribution of higher-order scattering processes becomes dominant.¹³ Furthermore, even for those regions where higher-order processes are less prominent, there have been no detailed assessments of the accuracy of the Born approximation as a function of relevant disorder parameters such as the penetration depth of the potential fluctuations and their correlation length along the wire axis. While the adiabatic approximation¹⁴ is expected to have somewhat broader applicability so long as intersubband scattering processes can be neglected, the reliability of that approach in a wide variety of conditions occurring in disordered quantum wires has not been critically tested either. Insofar as interface roughness scattering will ultimately govern the low-temperature mobilities attainable in quantum wires, a more careful examination of this issue seems warranted. It will be seen that our investigation of a system with fewer degrees of freedom also provides useful insights into the nature of the interface roughness scattering process for the case of narrow quantum wells, since thus far even that problem has not been treated in full generality. The important role of multisubband transport will be particularly emphasized, and we also demonstrate that our approach provides a useful means for examining localization phenomena.

II. BORN AND ADIABATIC APPROXIMATIONS

Before proceeding to describe our basic approach to 2D transport, let us briefly review the most common existing

methods for calculating momentum relaxation for electrons in disordered quantum wires. The stationary states of disordered wires have been studied by Taylor *et al.*¹⁵ and Singh,¹⁶ who concluded that a moderate amount of lateral disorder does not alter the qualitative characteristics of the density of states (DOS) profile for the lower electron subbands. Nixon and co-workers studied the effect of employing realistic self-consistent potentials, e.g., due to randomly positioned ionized donors, on the quantized resistance in point contacts.^{17,18} The importance of correctly treating structural disorder in quantum-dot nanostructures was pointed out by Jovanovic *et al.*¹⁹

Here we are interested primarily in finding the interface roughness scattering rate, a task that has usually been accomplished using the first-order perturbation theory as embodied in the Born approximation. In calculating the scattering rate for electrons propagating along the wire axis (\hat{z}), we will only be concerned with 1D quantum confinement along the \hat{y} axis, i.e., the confinement in the growth direction \hat{x} is assumed to be much stronger than along \hat{y} , and does not contribute fluctuations as a function of lateral position. This makes the problem computationally manageable without loss of generality. Assuming that the roughness in the wire of width W is characterized by the fluctuation height Δ along the \hat{y} axis and the lateral size Λ along the \hat{z} axis, Gaussian roughness can be described by the following autocorrelation function:

$$\langle \Delta(z)\Delta(z') \rangle = \Delta^2 \exp\left(-\frac{|z-z'|^2}{\Lambda^2}\right). \quad (1)$$

The momentum relaxation rate within the Born approximation is proportional to the Fourier transform of the autocorrelation function. If intrasubband scattering alone is significant, only backward scattering is allowed by momentum (k) conservation, and the relaxation rate takes the following form:

$$\frac{1}{\tau_R(k)} = \frac{2\sqrt{\pi}\Lambda(\delta E)^2 m^*}{\hbar^3 k} \exp(-\Lambda^2 k^2), \quad (2)$$

where m^* is the effective mass, δE is the fluctuation in the quantization energy corresponding to the jump in the wire width (for an infinite barrier in one dimension $\delta E = -\pi^2 n^2 \hbar^2 \Delta / m^* W^3$, $n=1,2,\dots$, and the factor of 2 accounts for the possibility of scattering from either of the two walls. It is implicitly assumed that the wire is sufficiently wide for the fluctuations at both walls to have an additive effect on the scattering rate. This discussion neglects electron screening of the potential fluctuations, which warrants a separate investigation.

If the Fermi energy $E_F = \hbar^2 k^2 / 2m^*$ for a parabolic band with an isotropic effective mass approaches or exceeds the energy of a higher electron subband, an appreciable fraction of the electrons comes to occupy the higher subband. The relaxation rate in the Born approximation for electrons starting out in the lower subband is determined primarily by the intersubband scattering rate. Both backward- and forward-scattering processes are allowed, and must be weighted in the final sum by the $(1 - k_f/k_i \cos\theta)$ factor, where $\theta = \pi$ and $\theta = 0$, respectively, k_i is the initial momentum, and k_f is the

final momentum. The expression for the relaxation rate is similar to Eq. (2), apart from using the product of the energy fluctuations in the two subbands in the numerator and $k_i - k_f$ instead of $2k$ in the exponent.^{20,21} The relaxation time calculated in this fashion is longer than that given by intrasubband scattering in the higher subband, but substantially shorter than that given by intrasubband scattering in the lower subband. Once the relaxation time for electrons at a given k value is estimated for each subband, the contribution to the relaxation time at the Fermi energy can be evaluated by solving for the subband energies and their fluctuations due to the disorder at the wire walls, and then finding the DOS for each subband using the Gaussian line shape with width δE .^{16,22} For an infinitely long wire in the absence of broadening, the DOS in a 1D system follows the well-known inverse square-root behavior with a singularity at the bottom of the subband. The roughness-limited mobility at a finite temperature is then given by $\mu_{\text{IR}} = e/m^* \langle \tau_R \rangle$, where

$$\langle \tau_R \rangle = \int \sum_j \tau_R^j(E) D_j(E) E \frac{\partial f_0(E)}{\partial E} \times dE \bigg/ \int \sum_j D_j(E) E \frac{\partial f_0(E)}{\partial E} dE, \quad (3)$$

where $D_j(E)$ is the density of states in subband j , and $f_0(E)$ is the Fermi-Dirac distribution function.

Kawabata¹³ showed that when $\Lambda k \gg 1$, the second-order contribution to the scattering rate obtained from perturbation theory exceeds the lowest-order contribution represented by Eq. (2). This region, however, corresponds to the condition of very slow fluctuations of the potential barriers, for which the adiabatic approximation is applicable.¹⁴ The main assumption of the adiabatic approximation is that the electron wave function $\Psi(y,z)$ in the time-dependent 2D Schrödinger equation:

$$\left[\frac{-\hbar^2}{2m^*} \left(\frac{\partial^2}{\partial y^2} + \frac{\partial^2}{\partial z^2} \right) + V(y,z) \right] \Psi(y,z,t) = i\hbar \frac{\partial \Psi(y,z,t)}{\partial t}, \quad (4)$$

where the potential $V(y,z)$ accounts for both the wire's confining potential, and the fluctuations in its width can be rewritten in terms of the local eigenfunction $\varphi_n(y,z)$: $\Psi(y,z,t) = \sum_n \psi(z,t) \varphi_n(y,z)$, which is the solution of the following equation:²¹

$$\left[\frac{-\hbar^2}{2m^*} \frac{\partial^2}{\partial y^2} + V(y,z) \right] \varphi_n(y,z) = U_n(z) \varphi_n(y,z). \quad (5)$$

Here $U_n(z)$ is the local energy eigenvalue for subband n . The time-dependent Schrödinger equation then takes on a simplified 1D form for any given subband,

$$\left[\frac{-\hbar^2}{2m^*} \frac{\partial^2}{\partial z^2} + U_n(z) \right] \psi(z,t) = i\hbar \frac{\partial \psi(z,t)}{\partial t}. \quad (6)$$

From the many alternative approaches to solving this equation for a given potential, in this paper we employ a numerical solution based on a finite-difference expansion of the second-derivative term.²³

$$\frac{\partial^2 \psi}{\partial z^2} \rightarrow \delta_z^2 \psi_j = \frac{\psi_{j+1} - 2\psi_j + \psi_{j-1}}{(\Delta z)^2}, \quad (7)$$

where Δz is the position increment along the \hat{z} axis, and ψ_j represents the value of the eigenfunction at a point $z = j\Delta z$. In this approach, an implicit differencing scheme for the effective Hamiltonian $H = -(\hbar^2/2m^*)\partial^2/\partial z^2 + U_n(z)$ is used:

$$\left(1 + \frac{i\delta t H}{2\hbar}\right) \psi_j^{n+1} = \left(1 - \frac{i\delta t H}{2\hbar}\right) \psi_j^n, \quad (8)$$

where δt is the time increment, ψ^n represents the value of the eigenfunction at the current time step, and ψ^{n+1} the eigenfunction value at the next time step. The latter can then be found by inverting a tridiagonal matrix with position indices. For details of the solution method and expected accuracy of the approximation, see Ref. 23.

Since the explicit assumption of the adiabatic approximation is that the electrons remain in the same subband, it is not possible to incorporate intersubband scattering without stepping beyond the confines of the adiabatic approximation (an outline of how such a calculation can be performed in the basis of adiabatic eigenstates can be found in Ref. 21).

III. 2D NUMERICAL APPROACH TO QUANTUM TRANSPORT

While the Born approximation offers a simple analytical solution and the adiabatic approximation provides at least qualitatively reasonable results for intrasubband scattering, under the conditions of interest for disordered wires, both sacrifice details of what is fundamentally a 2D rather than 1D problem. Instead of making the adiabatic approximation and considering the electron propagation along the wire in terms of local eigenstates, we now discuss a more general approximation of the full 2D Schrödinger equation [Eq. (4)]. Several techniques for computing the electron dynamics in multiple dimensions have been reported in the literature.^{24–26} In our study, we will employ an approach that is analogous to the numerical calculation in the adiabatic approximation.²⁷ One of the advantages of this scheme is the possibility of extending it to include the effects of weak dissipation,²⁸ although this extension is beyond the scope of this work. Making use of the implicit differencing scheme [Eq. (7)] that preserves the unitarity of the evolution operator, we can bring the 2D equation into the following form:

$$\begin{aligned} & \left(1 - \frac{i\delta_y^2}{\lambda}\right) \left(1 - \frac{i\delta_z^2}{\lambda}\right) \exp(i\delta t V_{j,m}/2\hbar) \psi_{j,m}^{n+1} \\ & = \left(1 + \frac{i\delta_y^2}{\lambda}\right) \left(1 + \frac{i\delta_z^2}{\lambda}\right) \exp(-i\delta t V_{j,m}/2\hbar) \psi_{j,m}^n, \end{aligned} \quad (9)$$

where $\lambda = 4m^*/\hbar^2 \delta t$. The key simplification comes from introducing an intermediate value $\psi_{j,m}^{n+1/2}$ for mathematical convenience. The intermediate value has no separate physical significance but allows the complex 2D problem [Eq. (9)] to be split into two tractable locally 1D equations:

$$\left(1 - \frac{i\delta_y^2}{\lambda}\right) \psi_{j,m}^{n+1/2} = \left(1 + \frac{i\delta_z^2}{\lambda}\right) \psi_{j,m}^n, \quad (10)$$

$$\begin{aligned} & \left(1 - \frac{i\delta_z^2}{\lambda}\right) \exp(i\delta t V_{j,m}/2\hbar) \psi_{j,m}^{n+1} \\ & = \left(1 + \frac{i\delta_y^2}{\lambda}\right) \exp(-i\delta t V_{j,m}/2\hbar) \psi_{j,m}^{n+1/2}. \end{aligned} \quad (11)$$

The right-hand side of Eq. (10) can be immediately evaluated since $\psi_{j,m}^n$ is known from either the initial conditions or the previous iteration. The left-hand side represents a tridiagonal matrix in indices along the \hat{y} axis, and can be readily solved using the Thomas algorithm.²⁹ Equation (11) can be handled in a similar manner, multiplying the wave function before and after the matrix inversion by $\exp(-i\delta t V/2\hbar)$.

The finite-difference scheme given by Eqs. (10) and (11) requires the initial condition at $t=0$, as well as boundary conditions for $y=0$, $z=0$, $y=y_{\max}$, and $z=z_{\max}$. To fix the boundary conditions, it is sufficient to assume that the wave function goes to zero at the edges of the simulation region. Since the potential fluctuations due to interface roughness are much smaller than the barrier potential, it is convenient to start with the product of a 1D Gaussian wave packet with the eigenfunction for a certain subband i in the unperturbed quantum wire:

$$\Psi(y, z, t=0) = \varphi_i(y) \left(\frac{2}{\pi\sigma^2}\right)^{1/4} \exp\left[ikz - \frac{(z-z_0)^2}{\sigma^2}\right]. \quad (12)$$

If necessary, a DOS-based combination of the initial subband profile can be included in place of $\varphi_i(y)$. However, it is easier to interpret the results in terms of a unique momentum relaxation time, if the entire wave packet is in the same subband. In a perfect quantum wire, this wave packet will propagate without scattering at a group velocity of $\hbar k/m^*$ from the starting center position z_0 . It is important to choose the width of the wave packet probability density $\sigma/2$, so that the momentum uncertainty $\Delta k = \sigma^{-1}$ is much smaller than the initial momentum k . At some future time t , the unscattered wave packet will be described by

$$\begin{aligned} \Psi(y, z, t) & = \varphi_i(y) \left(\frac{2\sigma^2}{\pi}\right)^{1/4} \frac{e^{i\phi}}{(\sigma^4 + 4\hbar^2 t^2/m^{*2})^{1/4}} \\ & \times \exp\left[ikz - \frac{(z - \hbar kt/m^*)^2}{\sigma^2 + 2i\hbar t/m^*}\right], \end{aligned} \quad (13)$$

where $\phi = -(\tan^{-1} 2\hbar t/m^* \sigma^2)/2 - \hbar k^2 t/2m^*$. Therefore, the simulation region must be made sufficiently large so that after the largest time of interest t_{\max} it easily accommodates the necessary multiple (typically, 4–5) of the width of the broadened wave packet $(\sigma/2) \sqrt{1 + 4\hbar^2 t_{\max}^2/m^{*2} \sigma^4}$ following propagation to the center position $\hbar kt_{\max}/m^* + z_0$.

The foregoing equations are applicable to any 2D potential profile. For simplicity, the barrier potential is taken to be of the same magnitude everywhere. To preserve the stability of the finite-difference scheme and allow for Δx , $\Delta y = 10 \text{ \AA}$, so that the discretization error does not accumulate with the passage of time,^{23,27} it is convenient to

choose $V_0 = 0.25$ eV. This potential is high enough to prevent electrons with the Fermi energies considered here from escaping from the quantum wire. The mesh point separations have been chosen to assure the convergence of the results for the relaxation time, and to reproduce adequately the correlation length for the potential fluctuations along the wire axis. For simplicity we will also assume binary interface fluctuations, such that the position of each wall can be only $Y(z) = Y_0 + \Delta/2$ or $Y(z) = Y_0 - \Delta/2$, where Y_0 is the unperturbed value, and $V(y, z) = 0$ for $|y| \leq Y(z)$ and $V(y, z) = V_0$ for $|y| > Y(z)$. Thus, in order to obtain numerically a disordered profile with correlation length Λ , it is sufficient to select a random number from a uniform distribution between -1 and 1 independently for each point along the wire axis, and to perform a convolution of the resulting random profile with a Gaussian line of width Λ . If the resulting real number associated with each point along the z axis is positive, a $Y_0 + \Delta/2$ fluctuation is taken; otherwise, the wall position becomes $Y_0 - \Delta/2$. The same procedure is repeated for the second wall, and wires with different potential profiles are obtained by generating distinct quasirandom number sequences. In our approach, resembling a Monte Carlo-type simulation, we perform the same calculation for a large number of wires with different randomly generated disordered potential profiles in order to extract a realistic average value of the momentum relaxation time. The technique could be straightforwardly extended to arbitrary fluctuations of the wire walls, be they discrete or continuous in the magnitude of the potential $V(y, z)$ or in the wire width $2Y(z)$. Furthermore, arbitrary shapes, e.g., in incorporating bends, branches, or T stubs, are easily accommodated, primarily at the expense of larger matrices and longer computation times.

The outlined numerical generation of disordered potential profiles is particularly convenient in the present case, since for the same series of randomly generated wires it permits a direct comparison between results of the 2D and adiabatic 1D calculations. In the latter, the potential profile $V(y, z)$ can be converted into the adiabatic eigenvalues $U_n(z)$ corresponding to different subbands n by solving for the quantization energies of the potential at each point z as shown by Eq. (6). Then the relaxation time for both 2D and 1D calculations can be obtained by following the evolution of the electron wave packet, performing Fourier transforms of the spatial distribution of the probability density at arbitrary intervals, and recording the value of the average momentum. Assuming an exponential decay of the average momentum as a function of time, it is possible to recover an averaged value of the relaxation time from the simulation results. One must be careful to follow the evolution only so long as scattering from the hard interfaces at the edges of the simulation region along the \hat{z} axis is negligible, so that spurious contributions from elastic reflections may be avoided. Reflections from the edge of the simulation region toward which the electron wave packet is moving can be eliminated by translating the boundary of the simulation frame forward at the velocity corresponding to the center momentum of the wave packet, since scattering due to interface roughness is rarely into a significantly greater forward momentum. On the other hand, since there is significant backward scattering, reflections from the back edge can be eliminated only by extending the length of the simulation region.

Because of this requirement and due to the large number of consecutive simulations necessary to obtain a converging average value of the momentum relaxation time, the 2D simulation usually followed the wave packet for only ≈ 500 fs. However, in cases, where convergence could not be achieved by that point, it was followed for as long as it was necessary to recover converging results. The extracted relaxation times nearly always increased gradually at first, and then saturated at some level. The initial scattering rate is greater because the profile assumed for the starting wave packet along the \hat{y} axis [Eq. (12)] does not represent an eigenstate for any particular point along the wire, but rather an averaged distribution for the entire wire length. In cases where multiple subbands are occupied in equilibrium, our assumption that all electrons being in the lowest subband also leads initially to an artificially high scattering rate.

Since the relaxation times obtained for most of the cases reported in this paper are significantly greater than 500 fs, strictly speaking our results should be viewed in terms of a scattering rate for the wave packet with a given initial momentum, rather than as a true relaxation time applying to time scales on the order of the momentum decay constant. By the time the initial momentum has decayed appreciably, secondary scattering of those portions of the wave packet that have already been scattered at least once plays a significant role. This does not limit our testing of the accuracy of the Born and adiabatic approximations, since both can similarly be used to generate scattering rates. It should also be emphasized that it is straightforward to obtain a true relaxation time using our technique as long as one is willing to commit the somewhat greater computational resources that would be required. We also note that whereas the various subbands are decoupled in the adiabatic approximation, the intersubband interactions arise automatically in the 2D calculation.

IV. RESULTS

We first consider a GaAs wire of width $W = 100$ Å, for which the energy separation between the first and second subbands is ≈ 93.0 meV. The disorder correlation length is assumed to be $\Lambda = 30$ Å, and the penetration depth is taken to be $\Delta = 10$ Å, which yields fluctuations in the quantization energy for the first and second subbands of 4.9 and 17.5 meV, respectively. This test case, with a value of Δ that is only 10% of the wire width, is more indicative of future trends than current technology, since recent experimental studies of quantum wires fabricated by electron-beam lithography and wet chemical etching have reported fluctuations of up to ± 30 Å in wires with widths as narrow as 100 Å.⁵

Momentum relaxation times for the full 2D simulation, adiabatic approximation, and Born approximation (one curve including only intrasubband scattering and the other both intrasubband and intersubband processes) for electron energies not too far away from the bottom of the lowest subband are presented in Fig. 1. Results for the numerical 2D and 1D calculations are not extended to very low Fermi energies, since the low momenta involved necessitate very broad wave packets, which in turn require substantially increased simulation times and larger spatial regions to obtain a reliable estimate of the relaxation time. Also, parts of the electron

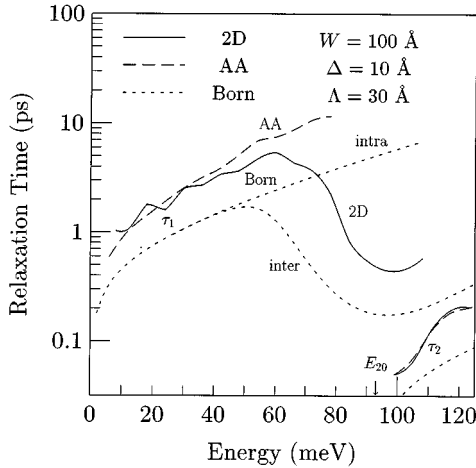


FIG. 1. Relaxation times for the lower two subbands as a function of electron energy as measured from the bottom of the first subband for a quantum wire with a 100-Å width and a 10-Å-thick disordered layer with a 30-Å correlation length. Results are given for the 2D calculation (solid curves), the 1D adiabatic approximation (dashed curves), and the Born approximation (dotted curves). In the case of the Born approximation for the first subband, scattering rates both with and without intersubband scattering processes are shown.

wave packet tend to become localized at very low energies, as discussed in connection with Fig. 6. The jagged appearance of the 2D curve for energies below 60 meV is an artifact due to uncertainties in estimating the saturation value for the relaxation time, since there is a relatively narrow temporal window between the onset of saturation and the onset of distortion due to secondary scattering. In this energy range the adiabatic approximation for the first subband shows a very good agreement with the 2D simulation. The Born approximation result also has a slope close to that of the 2D curve, although its magnitude is too small by a factor of ≈ 2.2 . This disagreement does not appear to be a consequence of assuming that the scattering from the two-wire interface is additive, since the ratio of the relaxation times obtained assuming disorder along one interface only produces a similar discrepancy.

The reduction in the relaxation time at energies above ≈ 60 meV for the 2D simulation with electrons starting out in the first subband, as well as for the Born approximation including intersubband scattering, corresponds to the onset of scattering to states in the second subband with a band minimum of ≈ 93 meV (indicated by an arrow in Fig. 1), which in the 2D simulation is broadened automatically by the potential fluctuations. Scattering to the second subband dominates τ_1 at higher energies due to both the higher DOS and the larger scattering rate [e.g., see Eq. (2)] at the bottom of that subband. Note also that after an intersubband scattering process, electrons may continue to move forward, as discussed for ionized impurity scattering in quantum point contacts.³⁰ The adiabatic approximation fails in the regime by producing scattering rates for electrons in single noninteracting subbands. The top end of the energy range is limited at 110 meV in order to minimize the probability of electrons escaping the walls of the quantum wire into the higher-potential barrier region in the 2D calculation. In the corre-

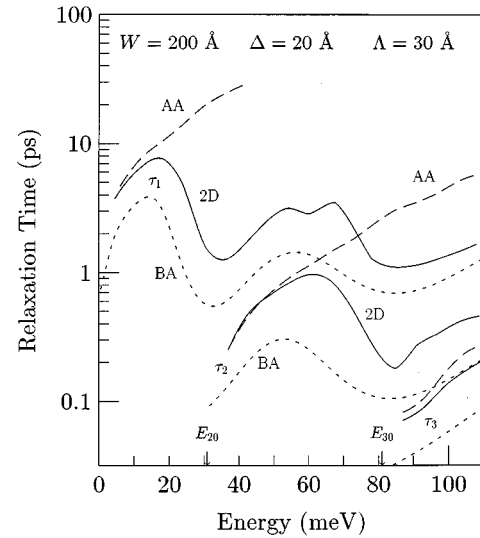


FIG. 2. Relaxation times for the lower three subbands as a function of electron energy as measured from the bottom of the first subband for a quantum wire with a 200-Å width and a 20-Å-thick disordered layer with a correlation length of 30 Å, for the 2D calculation (solid), 1D adiabatic approximation (dashed), and Born approximation (dotted).

sponding calculation for electrons initially in the second subband, the adiabatic approximation yields excellent agreement with the 2D results, while the Born approximation again produces an underestimate for the relaxation time (see the curves for τ_2 in the lower-right-hand-side corner of Fig. 1). We find that as long as intersubband scattering is incorporated, the Born approximation reproduces the correct qualitative features for both subbands, even though there is a factor of 1.5–5 of quantitative discrepancy at all energies.

While the quantum wire with a lateral width of 100 Å is particularly well suited for studying 1D quantum effects, since its first-to-second subband separation is much greater than the thermal energy at room temperature, at present such lateral dimensions are rather difficult to realize experimentally. To provide a better illustration of a more accessible structure in which multiple subbands come into play over most of the energy range of interest, Fig. 2 shows analogous results for a 200-Å-wide quantum wire with the same correlation length and boundary fluctuations still equal to 10% of its width. Here the separations between the first and second and the first and third subbands are 30.9 and 81.0 meV, respectively, and, for $\Delta = 20$ Å, the fluctuations in the quantization energy are 1.8, 7.0, and 15.2 meV, respectively. The general trends are similar to those in Fig. 1. Note that the relaxation times for electrons starting in the first three subbands are shown for all methods of calculation. The adiabatic approximation is again within 10% of the 2D results for the first subband, until the onset of intersubband scattering, which occurs at much smaller energies, while relaxation times obtained with the Born approximation are a factor of 1.9 smaller. At any given energy, the relaxation times are somewhat longer than in Fig. 1, since the fluctuations in the quantization energy are weaker in the wider wire. Furthermore, scattering to the third subband at 81.0 meV now produces a second dip in the relaxation time. The behavior of the curve for electrons in the second subband is similar to

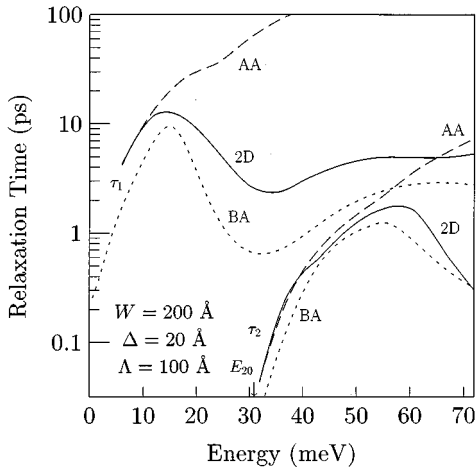


FIG. 3. Relaxation times for the lower two subbands as a function of electron energy as measured from the bottom of the first subband for a quantum wire with a 200-Å width and a 20-Å-thick disordered layer with a correlation length of 100 Å, for the 2D calculation (solid), 1D adiabatic approximation (dashed), and Born approximation (dotted).

that for the first, although the numerical value of the relaxation time is smaller due to the increased magnitude of the potential fluctuations.

Figure 3 shows the effects of increasing the correlation length to $\Lambda = 100$ Å, while holding the other parameters the same as in Fig. 2. The slope of each curve near the bottom of a subband increases, as should be expected from the Λ dependence of the scattering rate exponent. For scattering in the first subband, the adiabatic approximation again gives excellent agreement with the 2D results, while the Born approximation results are smaller by a factor of ≈ 2.2 . The 2D curve for the first subband remains almost flat beyond ≈ 45 meV, whereas the relaxation time for the second subband drops substantially to indicate the onset of scattering to the third subband. While the Born approximation is usually thought of as predicting a substantial increase of the relaxation time at higher energies due to an exponential dependence on the $k\Lambda$ product [see Eq. (2)], we find that this enhancement does not materialize when the effects of the higher subbands are properly accounted for.

In all of the cases considered above, the 1D adiabatic calculation produced a reasonably good approximation of the full 2D results as long as the electron energy was low enough that higher-subband processes could be ignored. Since the reduction of the computational approach to 1D yields a substantial savings in the computer time, it is of great interest to determine whether that agreement extends to other values of correlation length and disorder penetration depth. To assure that only intrasubband processes are operative, we consider the 100-Å-wide wire and a fixed Fermi energy of 42 meV. This energy is well below the onset of scattering to the second subband, yet large enough to facilitate convergence of the numerical results for simulations with different random potential profiles. For a fixed disorder penetration depth of 10 Å, the momentum relaxation times as a function of correlation length for the 2D, adiabatic, and Born calculations are shown in Fig. 4. The smallest correlation length of 15 Å is limited by the requirement that the island size along the

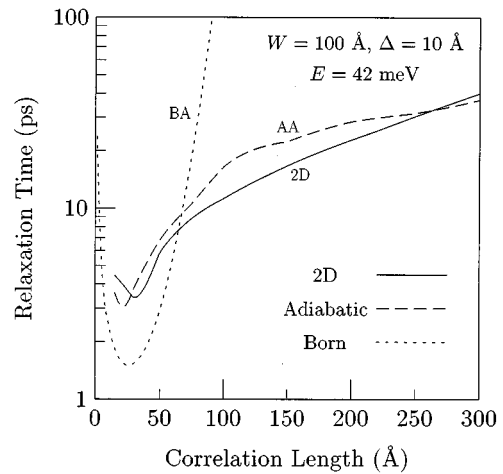


FIG. 4. Relaxation times as a function of disorder correlation length for a quantum wire with a 100-Å width and a 10-Å-thick disordered layer. Results are shown for an electron Fermi energy of 42 meV using the 2D calculation (solid), 1D adiabatic approximation (dashed), and Born approximation (dotted).

wire axis reproduces the correlation length accurately in the discretized version of the potential profile, since very small islands require very long simulation times. From Fig. 4, it can be observed that the adiabatic approximation agrees with the 2D results to within 50% for the entire range of correlation lengths considered, and in some regions the agreement is much better. For correlation lengths between 20 and 50 Å, the relaxation time obtained within the Born approximation is too low by a substantial factor (as much as 2.5); however, it cannot be ruled out that the agreement is much better for uncorrelated disorder ($\Lambda \rightarrow 0$). At very small correlation lengths, the Born approximation relaxation time increases due to domination by the linear Λ term in the expression for the relaxation rate. The 2D and 1D adiabatic results show a similar relaxation time minimum at small Λ , which is, however, not as deep as the minimum predicted by the Born approximation. In the opposite limit of long correlation lengths, the Born relaxation time increases exponentially, reaching 360 ps at $\Lambda = 100$ Å. However, the more reliable 2D and adiabatic results indicate that this is unphysical, since higher-order scattering processes dominate.¹³ The 2D and adiabatic results agree well in this regime, as expected from the definition of the adiabatic approximation; however, accurate numerical results are more difficult to recover since averages over longer disordered potential patterns are required.

For fixed correlation lengths of 30 and 100 Å and the same wire width (100 Å) and electron energy (42 meV) as in Fig. 4, momentum relaxation times in the various approximations are shown in Fig. 5 as a function of disorder penetration depth. While it should be clear from the discussion following Eq. (2) that the relaxation time in the Born approximation is inversely proportional to Δ^2 when the barriers are infinite, the dependence is slightly subquadratic for the present case of high yet finite barriers. The slope as a function of Δ for the Born approximation is nearly identical to that for the adiabatic and 2D results presented in Fig. 5. However, for $\Lambda = 30$ Å, the Born approximation result is smaller than that from either numerical approach by a factor decreasing from 2.7 at $\Delta = 2.5$ Å to 1.9 at 20 Å. On the other

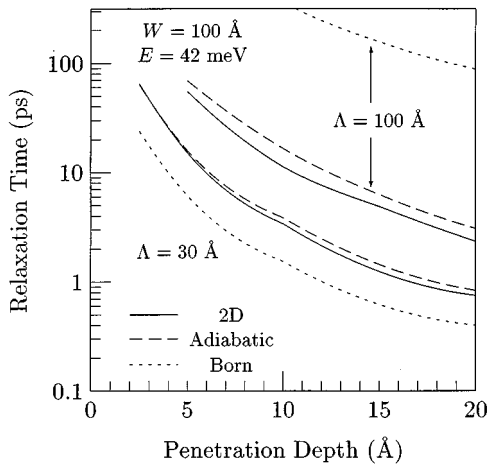


FIG. 5. Relaxation times as a function of disorder depth for a quantum wire with a 100-Å width and a 30-Å disorder correlation length. Results are shown for an electron Fermi energy of 42 meV using the 2D calculation (solid), 1D adiabatic approximation (dashed), and Born approximation (dotted).

hand, for $\Lambda = 100$ Å, the Born approximation yields an order-of-magnitude *overestimate* of the relaxation time owing to the neglect of higher-order scattering processes, as shown in Fig. 4. The adiabatic approximation yields excellent agreement with the 2D result for $\Lambda = 30$ Å, while it overestimates the relaxation time at $\Lambda = 100$ Å by 25–50%. In both cases, the discrepancy is nearly independent of Δ .

An additional advantage of the 2D approach is that it allows us to probe the region where the electron kinetic energy is smaller than the fluctuations in the quantization energy. Under those conditions the wave packet cannot propagate freely along the wire axis, but instead tends to become confined to spatial regions with low potential energy. This case corresponds to the well-known class of localization phenomena.^{31,32} The distinguishing characteristic of the wave function associated with a localized electronic state is its exponential decay with distance from the probability maximum. Localized and extended stationary states are separated in energy by the mobility edge, below which electrons are confined by reflections from potential fluctuations with higher energies.³³ The localized states in quantum wires with a finite length can readily be determined from a multidimensional finite-difference solution of the time-independent Schrödinger equation.¹⁶ In the time-domain approach of this paper, localization can be observed as a function of time after the injection of the wave packet. In Fig. 6, the probability density at injection and at 20 ps after injection are shown for a 100-Å-wide quantum wire with a disorder correlation length of 30 Å and a disorder penetration depth of 20 Å. For comparison, the effective potential profile due to fluctuations of the quantization energy in the same disordered wire is also shown. It can be seen that the potential maxima at approximately 500 and 750 nm both exceed the wave-packet energy of 6 meV. This causes a large portion of the wave packet, which is not able to tunnel through the barrier at ≈ 750 nm, to undergo multiple reflections from the effective potential barriers at these points, and become localized for a substantial period of time ($\approx 40\%$ of the original probability remains in the simulation region after 20 ps). However, over

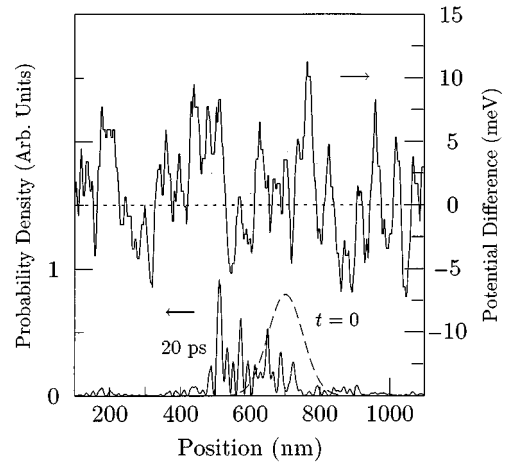


FIG. 6. Probability density as a function of position along the axis of a 100-Å-wide quantum wire for the injected wave packet with an energy of 6 meV (dashed curve), and its remainder after 20 ps (solid curve). The disorder penetration depth is 20 Å, and the correlation length is 30 Å. Also shown is the deviation of the quantization energy from its value in a perfect wire averaged over 200-Å intervals. The absorbing edges of the simulation region are located between 0 and 100 nm and 1100 and 1200 nm along the horizontal axis.

time the total probability in the effective potential well decays due to tunneling through the potential barriers. In obtaining Fig. 6, the parts of the wave packet penetrating to distances < 100 nm and > 1100 nm have been gradually eliminated by introducing a gently graded exponential reduction of the probability with time (absorbing boundary conditions).

V. DISCUSSION

We have performed a parametric study of quantum transport in disordered quantum wires using a 2D simulator of electronic wave-packet propagation. Momentum relaxation times obtained from this quite general formulation have been compared to results from the Born and adiabatic approximations in order to assess the reliability of those less computationally intensive approaches under a variety of conditions. Localization of portions of the wave packet has also been simulated for energies below the mobility edge.

For intrasubband roughness scattering, we find that the Born approximation tends to underestimate the relaxation time by about a factor of 2 for correlation lengths less than 30–40 Å, and to overestimate it by orders of magnitude for correlation lengths greater than 70 Å. On the other hand, in that regime, the adiabatic approximation reproduces the results of the full 2D calculation to within 50% for a wide range of wire sizes and disorder parameters. However, at energies large enough that intersubband processes play a role, neither approximation yields satisfactory quantitative agreement with the more general 2D results. Since the adiabatic approximation does not incorporate the effects of intersubband scattering, its predictions for higher electron energies result in a substantial overestimate of the momentum relaxation time.

In the present analysis, our 2D calculation was performed

for the case of a quantum wire with strong confinement and no thickness fluctuations in the third dimension. However, the conclusions of this work may have implications for interface roughness scattering in other quantum structures. For example, our finding that the Born approximation routinely underestimates the momentum relaxation time in disordered wires by about a factor of 2 whenever $k\Lambda < 1$ suggests that the common use of the Born approximation to calculate interface-roughness-limited mobilities in quantum wells may be inadequate if a precise quantitative result is needed. In particular, if the same correction factor is assumed to apply, it may account for the fact that the interface roughness correlation lengths extracted from a comparison of experimental low-temperature mobility data for GaAs/Al_xGa_{1-x}As quantum wells with Born approximation predictions (≈ 70 Å) (Ref. 34) tend to exceed the estimates based on photoluminescence excitation spectroscopy (< 30 Å).³⁵ While a direct verification of this using a 3D finite-difference approach analogous to the 2D formulation adopted here would be quite challenging from a computational standpoint, a 2D adiabatic approximation analogous to the 1D formulation discussed above might be relatively accurate as long as the energies of interest are low enough that intersubband processes may be ignored.

We emphasize again the generality of our basic approach, which may be applied to time-dependent quantum transport or localization in structures with any in-plane geometry, as long as the required grid size and time step are compatible with the available computational resources. For example, the response of mesoscopic electronic devices with large electric fields could be modeled. The method could also be generalized to treat magnetotransport and edge states in structures with high magnetic fields and arbitrary geometries. A separate work will discuss the development of a method for solving the time-dependent 2D Schrödinger equation for a time-varying Hamiltonian. This allows the treatment of time-varying fields as well as the inclusion of a harmonic potential to enable the modeling of phonon-scattering processes that dominate the electron transport at higher temperatures. Such

a technique may be used to extend the calculations of polar-optical phonon-scattering rates, which have already been discussed in the literature for perfect rectangular quantum wires,^{36,37} as well as for wires with interface roughness and for arbitrary three-dimensional geometries^{22,38} to situations where Matthiesen's rule and the relaxation-time approximation are inadequate. A different approach to this problem starting with the time-domain calculation of this paper is to include weak dissipation by phonon scattering via Monte Carlo sampling of the electron-phonon-coupled potentials.²⁸ It should also be noted that another important mechanism is scattering by randomly positioned ionized impurities, which can be treated using the approach presented in this paper once the self-consistent potential due to the scatterers is determined.¹⁸

It should finally be noted by way of comparison that Wigner function models, which were used some time ago to calculate the characteristics of resonant-tunneling diodes,^{39,40} are attractive, since dissipative phonon scattering can be straightforwardly incorporated (using, for example, a weighted Monte Carlo technique.⁴¹) However, the need to perform computations in momentum as well as real space renders the possibility of useful calculations for arbitrary 2D geometries unlikely in the absence of supercomputer resources. Another approach is to include the electron-phonon interaction into the treatment of quantum transport nonperturbatively using numerical real-time path-integral calculations.⁴² However, even for an oversimplified parabolic confinement potential, the calculations tend to be quite complex,⁴³ and an extension to arbitrary potentials may prove to require computational resources that are considerably greater than those used in this work.

ACKNOWLEDGMENTS

This work was supported by the Office of Naval Research, and was performed while one of the authors (I.V.) held a National Research Council-Naval Research Laboratory Research Associateship.

¹H. Sakaki, Jpn. J. Appl. Phys. **19**, L735 (1980).

²D. Gershoni, H. Temkin, C. J. Dolan, J. Dunsmuir, S. N. G. Chu, and M. B. Panish, Appl. Phys. Lett. **53**, 995 (1988).

³M. Kohl, D. Heitmann, P. Grambow, and K. Ploog, Phys. Rev. Lett. **63**, 2124 (1989).

⁴M. Notomi, M. Okamoto, and T. Tamamura, J. Appl. Phys. **75**, 4161 (1994).

⁵P. Ils, A. Forchel, K. H. Wang, Ph. Pagnod-Rossiaux, and L. Goldstein, Phys. Rev. B **50**, 11 746 (1994).

⁶M. Tsuchiya, J. M. Gaines, R. H. Yan, R. J. Simes, P. O. Holtz, L. A. Coldren, and P. M. Petroff, Phys. Rev. Lett. **62**, 466 (1989).

⁷A. Chavez-Pirson, H. Ando, H. Saito, and H. Kanbe, Appl. Phys. Lett. **64**, 1759 (1994).

⁸E. Kapon, D. M. Hwang, and R. Bhat, Phys. Rev. Lett. **63**, 430 (1989).

⁹A. C. Maciel, C. Keiner, L. Rota, J. F. Ryan, U. Marti, D. Martin, F. Morier-Gemoud, and F. K. Reinhart, Appl. Phys. Lett. **66**, 3039 (1995).

¹⁰S. Block, M. Suhrke, S. Wilke, A. Menschig, H. Schweizer, and D. Grützmacher, Phys. Rev. B **47**, 6524 (1993).

¹¹J. Motohisa and H. Sakaki, Appl. Phys. Lett. **60**, 1315 (1992).

¹²H. Sakaki, T. Noda, K. Hirakawa, M. Tanaka, and T. Matsusue, Appl. Phys. Lett. **51**, 1934 (1987).

¹³A. Kawabata, J. Phys. Soc. Jpn. **61**, 3220 (1992).

¹⁴L. I. Glazman, G. B. Lesovik, D. E. Khmel'nitskii, and R. I. Shekhter, Pis'ma Zh. Eksp. Teor. Fiz. **48**, 218 (1988) [JETP Lett. **48**, 238 (1988)].

¹⁵J. P. G. Taylor, K. J. Hugill, D. D. Vvedensky, and A. MacKinnon, Phys. Rev. Lett. **67**, 2359 (1991).

¹⁶J. Singh, Appl. Phys. Lett. **59**, 3142 (1991).

¹⁷J. A. Nixon and J. H. Davies, Phys. Rev. B **41**, 7929 (1990).

¹⁸J. A. Nixon, J. H. Davies, and H. U. Baranger, Phys. Rev. B **43**, 12 638 (1991).

¹⁹D. Jovanovic, J. P. Leburton, H. Chang, R. Grundbacher, and I. Adesida, Phys. Rev. B **50**, 5412 (1994).

²⁰H. Akera and T. Ando, Phys. Rev. B **43**, 11 676 (1991).

- ²¹A. Kawabata, J. Phys. Soc. Jpn. **62**, 3988 (1993).
- ²²I. Vurgaftman and J. Singh, Appl. Phys. Lett. **62**, 2251 (1993).
- ²³A. Goldberg, H. Schey, and J. L. Schwartz, Am. J. Phys. **35**, 177 (1967).
- ²⁴R. Kosloff, J. Phys. Chem. **92**, 2087 (1988).
- ²⁵F. Ancilotto, A. Selloni, L. F. Xu, and E. Tosatti, Phys. Rev. B **39**, 8322 (1989).
- ²⁶F. Ancilotto, A. Selloni, and E. Tosatti, Phys. Rev. B **40**, 3729 (1989).
- ²⁷I. Gailbraith, Y. S. Ching, and E. Abraham, Am. J. Phys. **52**, 60 (1984).
- ²⁸L. F. Register and K. Hess, Phys. Rev. B **49**, 1900 (1994).
- ²⁹A. R. Mitchell, *Computational Methods in Partial Differential Equations* (Wiley, New York, 1969).
- ³⁰M. J. Laughton, J. R. Barker, J. A. Nixon, and J. H. Davies, Phys. Rev. B **44**, 1150 (1991).
- ³¹P. W. Anderson, Phys. Rev. **109**, 1492 (1958).
- ³²N. F. Mott and W. D. Twose, Adv. Phys. **10**, 107 (1961).
- ³³N. F. Mott, *Conduction in Non-Crystalline Materials* (Oxford University Press, Oxford, 1987).
- ³⁴T. Noda, M. Tanaka, and H. Sakaki, Appl. Phys. Lett. **57**, 1651 (1990).
- ³⁵J. C. Woo, S. J. Rhee, Y. M. Kim, H. S. Ko, W. S. Kim, and D. W. Kim, Appl. Phys. Lett. **66**, 338 (1995).
- ³⁶J. P. Leburton, J. Appl. Phys. **56**, 2850 (1984).
- ³⁷K. W. Kim, M. A. Stroschio, A. Bhatt, R. Mickevicius, and V. V. Mitin, J. Appl. Phys. **70**, 319 (1991).
- ³⁸I. Vurgaftman, Y. Lam, and J. Singh, Phys. Rev. B **50**, 14 309 (1994).
- ³⁹W. R. Frensley, Phys. Rev. B **36**, 1570 (1987).
- ⁴⁰N. C. Klusdahl, A. M. Krizan, D. K. Ferry, and C. Ringhofer, Phys. Rev. B **39**, 7720 (1989).
- ⁴¹F. Rossi, P. Poli, and C. Jacoboni, Semicond. Sci. Technol. **7**, 1017 (1992).
- ⁴²B. A. Mason and K. Hess, Phys. Rev. B **39**, 5051 (1989).
- ⁴³C. C. Wan, Y. Huang, and H. Guo, Phys. Rev. B **53**, 10 951 (1996).